IEEE Access
Multidisciplinary | Rapid Review | Open Access Journal

SPECIAL SECTION ON ARTIFICIAL INTELLIGENCE FOR PHYSICAL-LAYER WIRELESS COMMUNICATIONS

Received October 27, 2019, accepted November 14, 2019, date of publication November 19, 2019,
date of current version December 5, 2019.

Digital Object Identifier 10.1109/ACCESS.2019.2954455

LFM Signal Analysis Based on Improved Lv Distribution

YU WANG[1], KE WANG[2], FULONG JING[3], XIAOYU LAN[1], (Member, IEEE), YAN ZOU[3], AND LIANGTIAN WAN[4], (Member, IEEE)

[1]College of Electronics and Information, Shenyang Aerospace University, Shenyang 110136, China
[2]National Demonstration Center for Experimental Electrical and Electronic Education, Yangtze University, Jingzhou 434023, China
[3]Shenyang Aircraft Design and Research Institute, Shenyang 110035, China
[4]School of Software, Dalian University of Technology, Dalian 116081, China

Corresponding author: Xiaoyu Lan (lanxiaoyu1015@163.com)

This work was supported by the National Science Foundation for Young Scientists of China under Grant 61801308.

ABSTRACT In this paper, we propose a parameter estimation method named improved Lv distribution (ImLVD) for linear frequency modulated (LFM) signals. In this method, based on the scaling principle, we present a two-scale estimation strategy to acquire low computational cost. The two-scale estimation strategy includes coarse estimation operation and fine estimation operation. To implement the strategy, improved scaled Fourier transform (ISFT) and Chirp-Z transform (CZT) operation are used, where the ISFT can be implemented by fast Fourier transform (FFT) and complex multiplications. By changing the frequency searching range of ISFT, the ISFT is used in different frequency ranges. To improve the anti-noise, we present an improved parameter selection criterion which can reduce the noise correlation effectively. In this paper, the implementation, anti-noise performance, and computational cost are analyzed. Through simulations and analyses, we demonstrate that the ImLVD outperforms the compared algorithms.

INDEX TERMS Linear frequency modulated (LFM) signals, parameter estimation, Lv distribution, two-scale estimation strategy.

I. INTRODUCTION

Signal processing is a very important research field [1]–[4], including the estimation of signal paramers [5]–[7]. Recently, analysis of LFM signals has received considerable attention. As a polynomial phase signal, the LFM signal can be processed by the methods mainly including time-frequency (TF) analysis methods and time-chirp rate (TCR) analysis methods.

Time-Frequency (TF) methods are divided into linear TF analysis methods and bilinear TF analysis methods. Linear TF analysis methods mainly include Short-time Fourier transform (STFT) methods [8]–[10] and local polynomial Fourier transform [11]. Bilinear TF analysis methods mainly include Wigner-Ville distribution (WVD) based methods [12], [13] and ambiguity function [14]. In order to solve the cross-term problem existing in bilinear TF methods, the Wigner-Hough transform [15], [16], Radon-Ambiguity transform [17], Hough-STFT [18], Hough-local polynomial periodogram [19], and Teager-Huang-Hough transform [20] are proposed. Although the TF analysis methods can be used to analyze LFM signal, several problems exist in these methods, including: (1) for the linear TF analysis methods, frequency and time resolution depends on the length of the window; (2) to suppress the cross-term, the Radon or the Hough Transform is performed which results in a large amount of computation; (3) anti-noise ability of the TF analysis methods is poor; (4) the parameters of LFM signal cannot be obtained directly. In addition to these TF methods, Fractional Fourier transform (FrFT) based methods [21], [22] are the special TF methods which attract more attention recently. However, the practical realization of the methods suffers the problem that the transform results cannot match to the continuous FrFT, and the parameter of the LFM signal cannot be obtained directly which is related with rotation angles.

Cubic phase function (CPF) [23] is an effective TCR analysis method for detecting and estimating the mono-component LFM signal, which can obtain the parameters directly. However, when dealing with multi-component LFM signals,

The associate editor coordinating the review of this manuscript and approving it for publication was Guan Gui.

this method has cross-term problem. To overcome the cross-term problem, product CPF (PCPF) [24] and integrated CPF (ICPF) [25] are proposed. By using the PCPF method, the cross-term problem can be avoided, but the energy of self-term is not fully utilized. By using the ICPF method, not only energy of the self-term is fully utilized but also the cross-term is suppressed. However, anti-noise ability of the ICPF is still poor. To overcome these problems, the coherently ICPF (CICPF) algorithm [26], [27] is proposed. By coherently integrating the energy of self-term, CICPF method improves the ability of cross-term suppression and enhances the signal-to-noise (SNR). Although estimation performance and identifiability of the CICPF are better than other CPF-based methods, the anti-noise ability of CICPF is still poor and computation of the CICPF is large.

In the reference [28], a simple and effective method named Lv's distribution (LVD) is proposed. Compared to the above methods, the LVD can be more easily implemented by using fast Fourier transforms (FFT), inverse FFT (IFFT), and complex multiplications. It is known that LVD can obtain good performance based on the analyses and simulations in [28] and [29]. Due to the excellent performance, the algorithm has been widely used in many fields [30]–[33]. However, the computation cost of LVD is still high for obtaining high precision estimation and the anti-noise performance is still poor because of the noise correlation [34].

In this paper, we propose a parameter estimation algorithm, known as improved Lv distribution (ImLVD), for noisy linear frequency modulated (LFM) signals. In the ImLVD, the two-scale estimation strategy is used to reduce the computational cost. To implement the strategy, the Chirp-Z transform (CZT) [35] and the improved scaled Fourier transform (ISFT) [36] are used. In the ISFT, by introducing a scaling factor, a new time variable is constructed to remove the coupling. Moreover, by changing the search range of frequency, the ISFT is used in different frequency ranges. The ISFT is implemented only by using FFT, IFFT, and complex multiplications. To improve the anti-noise performance, the proposed method proposes an improved parameter selection criterion.

The rest of paper is organized as follows. In Section 2, we review the principle of LVD. In Section 3, we give the principle and the implementation of proposed algorithm in detail. In Section 4, based on a few numerical examples, we demonstrates the effectiveness of the proposed algorithm. In Section 5, some concludes are given.

II. REVIEW OF LVD

The parameters of signals mainly include frequency [37] and direction-of-arrival [38]–[41]. In this paper, we only focus on research into the frequency parameters of LFM signal. We will give a briefly reviews of the LVD [28]. The representation of multi-component LFM signals is as follow:

$$s_m(t) = \sum_{i=1}^{Q} A_i \exp\left(j2\pi f_i t + j\pi\gamma_i t^2\right), \tag{1}$$

where $s_m(t)$ denotes the multi-component LFM signals, Q denotes the number of components, A_i is the constant amplitude, f_i and γ_i denote the centroid frequency and chirp rate, respectively. In the LVD, the authors define a parametric symmetric instantaneous auto-correlation function (PSIAF), the expression of PSIAF is

$$\begin{aligned} R_{s_m}(t,\tau) &= s_m\left(t+\frac{\tau+a}{2}\right)s_m^*\left(t-\frac{\tau+a}{2}\right) \\ &= \sum_{i=1}^{Q} A_i^2 \exp\left(j2\pi f_i(\tau+a) + j2\pi\gamma_i(\tau+a)t\right) \\ &\quad + \sum_{i=1}^{Q-1}\sum_{j=i+1}^{Q}\left(R_{s_{m,i}s_{m,j}}(t,\tau) + R_{s_{m,j}s_{m,i}}(t,\tau)\right), \end{aligned} \tag{2}$$

where a denotes a constant time-delay which is related to scaling operator. $R_{s_{m,i}s_{m,j}}$ and $R_{s_{m,j}s_{m,i}}$ denote cross-terms. Equation (2) shows that t and τ couple with each other. Due to the linear frequency migration, such a coupling leads to a blurred representation of the LFM signals on the two dimensional (2D) centroid frequency and chirp rate (CFCR) domain. To remove the coupling, the authors propose a scaling operator $\mathrm{H}[\cdot]$ which is defined by

$$\mathrm{H}[g(t,\tau)] \to g\left(\frac{t_n}{\rho(\tau+a)}, \tau\right), \tag{3}$$

where $g(\cdot)$ is the phase function of signal, ρ and t_n denote the scaling factor and scaled time, respectively. When the operator $\mathrm{H}[\cdot]$ is applied to (2), a new expression is obtained as follow:

$$\begin{aligned} &\mathrm{H}\left[R_{s_m}(t,\tau)\right] \\ &\quad = \sum_{i=1}^{Q} A_i^2 \exp\left(j2\pi f_i(\tau+a) + j2\pi\frac{\gamma_i}{\rho}t_n\right) \\ &\qquad + \sum_{i=1}^{Q-1}\sum_{j=i+1}^{Q}\mathrm{H}\left[R_{s_{m,i}s_{m,j}}(t,\tau) + R_{s_{m,j}s_{m,i}}(t,\tau)\right]. \end{aligned} \tag{4}$$

Equation (4) shows that the coupling existed in (2) is removed. The lag variable τ and the new time variable t_n are independence from each other. The LVD is obtained by performing 2D Fourier transformation (FT) on (4), which is represented by

$$\begin{aligned} L_{s_m}(f,\gamma) &= \mathrm{F}_\tau\left[\mathrm{F}_{t_n}\left[\mathrm{H}[R_{s_m}(t,\tau)]\right]\right] \\ &= \sum_{i=1}^{Q} L_{s_{m,i}}(f,\gamma) + \sum_{i=1}^{Q-1}\sum_{j=i+1}^{Q} L_{s_{m,i}s_{m,j}}(f,\gamma), \end{aligned} \tag{5}$$

where $\mathrm{F}_\tau[\cdot]$ denotes performing FT along the lag variable τ, and $\mathrm{F}_{t_n}[\cdot]$ denotes performing FT along the time variable t_n. The first term of (5) denotes the self-terms and the second term denotes the cross-terms. By using the LVD method, the LFM signals are accumulated as the peaks in the 2D CFCR domain. The parameters can be obtained by locating

the peaks. However, in practical applications, the computation cost of LVD is high for obtaining high precision estimation. Moreover, since the constant delay in PSIAF is selected by using the parameter selection criterion introduced in [28], the noise correlation is strong which leads to bad anti-noise performance [34].

III. IMLVD METHOD

In this section, based on mono- and multi-component LFM signal, we introduce the principle of ImLVD.

A. PEAK ACCUMULATION

According to the PSIAF in LVD, we defind an self-correlation function which is represented as

$$R_{s_m}(t,\tau) = s_m\left(t+\frac{\tau+D}{2}\right)s_m^*\left(t-\frac{\tau+D}{2}\right), \quad (6)$$

where D is a new constant delay which will be discussed in III-D. Substituting the multi-component LFM signals s_m in (6), we can obtain

$$R_{s_m}(t,\tau) = \sum_{i=1}^{Q} A_i^2 \exp\left(j2\pi f_i(\tau+D) + j2\pi\gamma_i(\tau+D)t\right) + R_{cross}. \quad (7)$$

where R_{cross} denotes the cross-terms. To estimate the parameters correctly, the coupling between t and τ should be removed. It is known that the similar coupling can be removed by using the keystone transform [30]. Inspired by the idea of keystone transform, we propose the ISFT-IFT operator in [36] which is expressed by

$$\begin{aligned} x(t_{new}) &= \mathrm{IFT}\left[\mathrm{ISFT}\left[x(t)\right]\right] \\ &= \mathrm{IFT}\left[\int_{-\infty}^{\infty} x(t)\exp\left(-j2\pi f_{t_{new}} t_{new}\right)d(t_{new})\right] \end{aligned} \quad (8)$$

where $t_{new} = \rho b t$. The purpose of b is to change t, and ρ denotes scaling factor. IFT[·] denotes inverse Fourier transform. The searching frequency $f_{t_{new}}$ is limited in the frequency range $[f_d, f_u]$, where f_d and f_u denote the lower limit and the upper limit, respectively. Therefore, the search frequency range can be controlled by changing f_d and f_u.

Replace $x(t)$ by $R_{s_m}(t,\tau)$ and set $b = (D+\tau)$. Then (8) is becoming

$$\begin{aligned} R_{s_m}(t_{new},\tau) &= \mathrm{IFT}\left[\mathrm{ISFT}[R_{s_m}(t,\tau)]\right] \\ &= \sum_{i=1}^{Q} A_i^2 \exp\left(j2\pi f_i(\tau+D) + j2\pi h_i t_{new}\right) \\ &\quad + \mathrm{IFT}[\mathrm{ISFT}(R_{cross}(t,\tau))], \end{aligned} \quad (9)$$

where $h_i = \gamma_i/\rho$ and $t_{new} = (D\rho + \tau\rho)t$. The purpose of D is to make sure $D\rho = 1$ and inherit advantages of the LVD, which will be discussed in III-D. Equation (9) shows that the coupling existed in $R_{s_m}(t,\tau)$ is removed. The peak is accumulated by performing two-dimension (2D) FT along the variable τ and the variable t_{new}, respectively, which is represented by

$$\begin{aligned} \mathrm{CFCR}\left(f_{t_{new}}, f_\tau\right) &= \mathrm{FT}_\tau[\mathrm{FT}_{t_{new}}[R_{s_m}(t_{new},\tau)]] \\ &= \mathrm{FT}_\tau[\mathrm{FT}_{t_{new}}[\mathrm{IFT}[\mathrm{ISFT}[R_{s_m}(t,\tau)]]]] \\ &= \sum_{i=1}^{Q} A_i^2 \exp(j2\pi f_i a)\delta(f_\tau - f_i)\delta(f_{t_{new}} - h_i) \\ &\quad + Q_{cross}(f_{t_{new}}, f_\tau), \end{aligned} \quad (10)$$

where $\mathrm{FT}_\tau[\cdot]$ and $\mathrm{FT}_{t_{new}}[\cdot]$ denote performing the Fourier transform along the variable τ and the variable t_{new}, respectively. CFCR is the 2D parameter domain. $Q_{cross}\left(f_{t_{new}}, f_\tau\right)$ is the cross-terms after performing peak accumulation operation.

Equation (10) shows that, by using the accumulation operation, self-term can be accumulated as a peak in CFCR domain. The coordinates of each peak are (f_i, h_i). Therefore, the parameters of LFM signal can be estimated by locating the peaks. It is noteworthy that γ_i can be obtained by $h_i = \gamma_i/q$. For the cross-term $Q_{cross}(f_{t_{new}}, f_\tau)$, it will be discussed in APPENDIX.

It is worth noting that, in (10), the IFT[·] and the $\mathrm{FT}_{t_{new}}[\cdot]$ operations can be removed because the IFT[·] operation is the inverse transformation of the $\mathrm{FT}_{t_{new}}[\cdot]$ operation. Thus, the peak accumulation technology, which is shown in (10), can be simplified to

$$\mathrm{CFCR}(f_{t_{new}}, f_\tau) = \mathrm{FT}_\tau[\mathrm{ISFT}_t[R_{s_m}(t,\tau)]]. \quad (11)$$

According to (11), we only need to perform the ISFT operation and the FT operation along the variable t and the variable τ to obtain the peak.

B. IMLVD WITH MONO-COMPONENT

In this subsection, the processing procedure of ImLVD is described based on a discrete mono-component LFM signal. Equation (1) is mono-component LFM signal when $K = 1$. Let T_s is the sampling interval, the discrete mono-component LFM signal is

$$s(n) = A\exp\left(j2\pi fnT_s + j\pi\gamma(nT_s)^2\right), \quad (1 \le n \le N_w), \quad (12)$$

where N_w is date length. Firstly, we will describe the implementation of ISFT, and then we will describe the parameter estimation process of mono-component LFM signal by using ImLVD.

1) IMPLEMENTATION OF ISFT

Based on the analysis in [28], [42], [43], we find that the ISFT can be implemented by using the CZT operation [35] because the CZT can change the frequency search range. The CZT is defined by

$$\mathrm{CZT}[s(n)] = \sum_{n=0}^{N-1} s(n) z_v^{-n} = \sum_{n=0}^{N-1} s(n) A^{-n} W^{nv}, \quad v = 0, 1, \cdots, V-1, \quad (13)$$

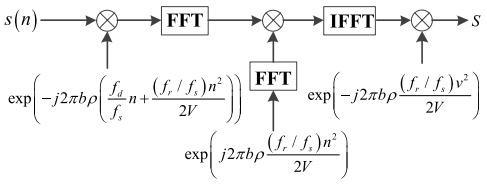

FIGURE 1. Flowchart of ISFT.

where V is the frequency number, both A and W are the arbitrary complex numbers with the forms $A = A_0 \exp(j\theta_0)$ and $W = W_0 \exp(-j\Delta_\phi)$. θ_0 denotes initial phase angle, W_0 denotes zooming factor, A_0 denotes initial radius length, and Δ_ϕ is the angle increment which is determined by frequency resolution.

For the ISFT, $W_0 = 1$ and $A_0 = 1$. To introduce the factor $b\rho$, the factors A and W should be set as

$$A = \exp\left(j2\pi \frac{f_d}{f_s} b\rho\right) \text{ and } W = \exp\left(-j2\pi \frac{f_r}{Vf_s} b\rho\right), \quad (14)$$

where f_s denotes the sampling frequency, $f_r = f_u - f_d$ is the selected frequency band. Substituting (14) in (13), the implementation of ISFT is defined as

$$\begin{aligned} \text{ISFT}\left[s\left(n\right)\right] &= \sum_{n=0}^{N-1} s\left(n\right) z_v^{-n} \\ &= \sum_{n=0}^{N-1} s\left(n\right) \exp\left(-j2\pi \left(\frac{f_d}{f_s} b\rho n + \frac{f_r}{Vf_s} b\rho n v\right)\right), \\ & \qquad v = 0, 1, \cdots, V-1. \end{aligned} \quad (15)$$

Inspired by the implementation of CZT, the implementation of ISFT is shown by Fig. 1.

Fig. 1 shows that the ISFT can be implemented by using FFT, IFFT, and multiplications. By changing f_d, f_u, and L, we can obtain different estimation precision.

2) PROCESSING PROCEDURE

The processing procedure is a two-step procedure. Firstly, we coarsely determine the frequency ranges of chirp rate and centroid frequency, this procedure is called coarse estimation operation. Secondly, we perform a fine search to accurately estimate chirp rate and centroid frequency, this procedure is called fine estimation operation.

According to the peak accumulation technique, we perform the self-correlation function on (12), and a $N \times N$ matrix is obtained which is expressed by

$$\mathbf{R_s} = \begin{bmatrix} R_s\left(n_1, m_1\right) & R_s\left(n_2, m_1\right) & \cdots & R_s\left(n_N, m_1\right) \\ R_s\left(n_1, m_2\right) & R_s\left(n_2, m_2\right) & \cdots & R_s\left(n_N, m_2\right) \\ \vdots & \vdots & \ddots & \vdots \\ R_s\left(n_1, m_N\right) & R_s\left(n_2, m_N\right) & \cdots & R_s\left(n_N, m_N\right) \end{bmatrix}, \quad (16)$$

where n_p denotes discrete time variable, and m_p denotes discrete lag variable, $1 \le p \le N$. $N = N_w - D/T_s$ denotes the effective signal length. By using the Claasen and Mecklenbrauker (CM) sampling criterion [12], the element in $\mathbf{R_s}$ is represented by

$$\begin{aligned} R_s\left(n_p, m_p\right) = A^2 \exp(&j2\pi f \left(2m_p T_s + D\right) \\ &+ j2\pi h \left(2\rho m_p T_s + D\rho\right) n_p T_s), \end{aligned} \quad (17)$$

where $h = \gamma/\rho$.

a: COARSE ESTIMATION

According to the analysis in Section III-A, we should perform the ISFT operation along time variable and perform the FT along lag variable to accumulate peak. For coarse estimation operation, FT is implemented by the FFT. Therefore, the peak accumulation processing is represented by

$$\text{CFCR}_1 = \text{FFT}_{\text{col}}\left[\text{ISFT}_{\text{row}}\left[\mathbf{R_s}\right]\right], \quad (18)$$

where $\text{ISFT}_{\text{row}}[\cdot]$ denotes performing the ISFT operation on the row vector, and $\text{FFT}_{\text{col}}[\cdot]$ denotes performing the FFT operation on the column vector. The coarse estimations of f and h, expressed as $\hat{f}$ and $\hat{h}$, are obtained by locating the peak in the CFCR_1 domain.

It is noteworthy that the searching frequency range of ISFT can be obtained by two criteria. Firstly, when the range of chirp rate has been known, and the range is $[f_{d,\gamma}, f_{u,\gamma}]$, so the upper limit and lower limit of ISFT are set to $f_d = f_{d,\gamma}/q$ and $f_u = f_{u,\gamma}/q$, respectively. Secondly, when the range of chirp rate is unknown, it is set to the maximum value under Nyquist frequency constraint, which means $f_d = -f_s/2, f_u = f_s/2$ in ISFT. In this paper, for coarse estimation operation, the range is unknown.

Setting the frequency number of the ISFT is L_1. Based on the CM sampling, the estimation precision of $\hat{f}$ and $\hat{h}$ are $f_s/2N$ and f_s/L_1, respectively. L_1 is decided by actual chirp rate resolution demand. When the resolution is unknown, the frequency number is set to $L_1 = N$. In order to improve estimation precision, we should perform fine estimation operation.

b: FINE ESTIMATION

For the fine estimation, to accumulate peak, FT is implemented by performing the CZT instead of FFT because we do not need to search entire frequency band. Thus, the fine estimation operation is expressed as

$$\text{CFCR}_2 = \text{CZT}_{\text{col}}\left[\text{ISFT}_{\text{row}}\left[\mathbf{R_s^C}\right]\right], \quad (19)$$

where $\text{CZT}_{\text{col}}[\cdot]$ denotes the CZT operation performing on the column vector, CFCR_2 denotes the CFCR domain which is obtained by performing fine estimation operation. We can estimate the fine estimations of $\hat{f}$ and $\hat{h}$ by locating the peak in the CFCR_2. The fine estimation of $\hat{\gamma}$ is obtained by $\hat{\gamma}^{fine} = \rho\hat{h}^{fine}$.

For the fine estimation operation, the searching frequency ranges of ISFT and CZT are selected around the coarse estimations $\hat{f}$ and $\hat{h}$, which is represented by

$$f_{r,f} = f_s/(2N) \text{ and } f_{r,h} = f_s/L_1, \quad (20)$$

where $f_{r,f}$ and $f_{r,h}$ denote the search frequency bandwidths of $\hat{f}$ and $\hat{h}$, respectively. In (20), $\frac{f_s}{2N}$ and $\frac{f_s}{L_1}$ are the estimation precision, which are obtained by the coarse estimation operation. Based on $f_{r,h}$ in (20), the factors of ISFT are set to

$$f_d = \hat{h} - f_{r,h}/2 \text{ and } f_u = \hat{h} + f_{r,h}/2. \tag{21}$$

The frequency number of ISFT is set to L_2.

Based on $f_{r,f}$ in (20), the factors of CZT are set to

$$\theta_0 = 2\pi \frac{\hat{f} - f_{r,f}/2}{f_s} \text{ and } \Delta_\phi = 2\pi \frac{f_{r,f}}{f_s L_{CZT}}, \tag{22}$$

where L_{CZT} is the frequency number.

Therefore, the final estimation precision of chirp rate and centroid frequency is $\frac{f_s}{2NL_{CZT}}$ and $\frac{f_s}{L_1 L_2}$, respectively. L_1, L_2 and L_{CZT} are the known parameters in advance, which are decided by practical requirement.

The steps of the proposed method are given as Algorithm 1.

Algorithm 1

1: Input: $s(n), f_s, L_1, L_2$, and L_{CZT}.
2: Step 1: Perform self-correlation function on $s(n)$ to obtain $\mathbf{R_s}$ based on (6).
3: Step 2: Set $f_d = -f_s/2$ and $f_u = f_s/2$ for ISFT. Perform ISFT and FFT on $\mathbf{R_s}$ to obtain CFCR_1 by (18).
4: Step 3: Search the peak in the CFCR_1 domain to obtain the coarse estimate parameters $\hat{f}$ and $\hat{h}$.
5: Step 4: Calculate the parameters of CZT and ISFT based on (20)-(22), and obtain CFCR_2 by (19).
6: Step 5: Get the fine estimation parameters $\hat{f}^{fine}$ and $\hat{h}^{fine}$ by searching the peak in CFCR_2, and calculate the fine estimation of chirp rate by $\hat{\gamma}^{fine} = q\hat{h}^{fine}$.
7: Output: The fine estimation parameters of LFM signal, $\hat{f}^{fine}$ and $\hat{\gamma}^{fine}$.

C. IMLVD WITH MULTI-COMPONENT

In this part, we discuss the proposed method for multi-component case. Based on (1), the discrete form of the multi-component LFM signals is represented by

$$s_m(n) = \sum_{i=1}^{Q} A_i \exp\left(j2\pi f_i n T_s + j\pi\gamma_i (nT_s)^2\right). \tag{23}$$

According to analysis in III-A, when we apply (11) on the multi-component LFM signals, there will be Q peaks in CFCR domain. Thus, after coarse estimation operation, Q peaks appear in CFCR_1. The coordinates of Q peaks are $\left\{\hat{f}_i, \hat{h}_i, i = 1, \cdots, Q\right\}$. Based on the coarse estimation, we set different parameters of CZT and ISFT for fine estimation operation. For example, for the ith peak, the parameters of CZT should be set to

$$\theta_{0i} = 2\pi \frac{\hat{f}_i - f_{r,f}/2}{f_s} \text{ and } \Delta\phi_i = 2\pi \frac{f_{r,f}}{f_s L_{CZT}}, \tag{24}$$

where θ_{0i} and $\Delta\phi_i$ denote the parameters of CZT of the ith component. The parameters of ISFT should be set to

$$f_{di} = \hat{h}_i - f_{r,h}/2 \text{ and } f_{ui} = \hat{h}_i + f_{r,h}/2, \tag{25}$$

where f_{ui} denotes the upper limit of searching frequency, and f_{di} denotes the lower limit of searching frequency. With the factors, we perform the fine estimation operation to accurately estimate the parameters of ith LFM signal. The parameters of other components are obtained by the same processing.

D. PARAMETER SELECTION

For the LVD, the constant delay greatly benefits its cross term suppression and anti-noise performance. According to the analysis in [28], the constant delay of LVD is set to "1s" whose purpose is to reduce the interpolation influence, but the anti-noise ability is still bad because of the noise correlation. In this paper, by using an improved parameter selection criterion, the anti-noise performance can be improved without increasing the influence of interpolation.

According to the analysis in [34], the constant delay is related to the anti-noise performance. When the constant delay is large, the noise correlation is small which is beneficial to improve the anti-noise performance. With the limitation of signal length, the anti-noise performance achieves its best when the constant delay is equal to the effective signal length [34]. So, in the (6), the constant delay is $D = NT_s$. According to the analysis of LVD, when no interpolation is required along the axis t_{new} and the interpolation on both sides of the t_{new} axis is symmetrical, the precision is the best.

Based on the analysis in (9), to remove the coupling, t is changed to a new variable t_{new} which is denoted by $t_{new} = (\rho D + \rho\tau)\, t$. By using the phase lines analysis method in [42], when $\rho D = 1$, there is no interpolation along the axis which is the same as the LVD. Thus, the selection of the parameters are expressed as

$$D = NT_s \text{ and } \rho = \frac{1}{NT_s}. \tag{26}$$

From (26), we can see that $\rho D = 1$.

IV. ANALYSIS OF ANTI-NOISE AND COMPUTATIONAL COST

In this section, the computational cost and the performance of anti-noise will be analyzed by using numerical simulations. According to the analysis in Introduction, the LVD and the CICPF are selected as the comparative methods.

A. ANTI-NOISE PERFORMANCE

The evaluation of anti-noise performance includes two parts, the mono-component LFM signal with noisy and the multi-component LFM signals with noisy.

1) MONO-COMPONENT LFM SIGNAL

According to the analysis methods geiven in [44] and [45], we use the input-output SNR to evaluate the anti-noise performance of the mono-component LFM signal. The amplitude,

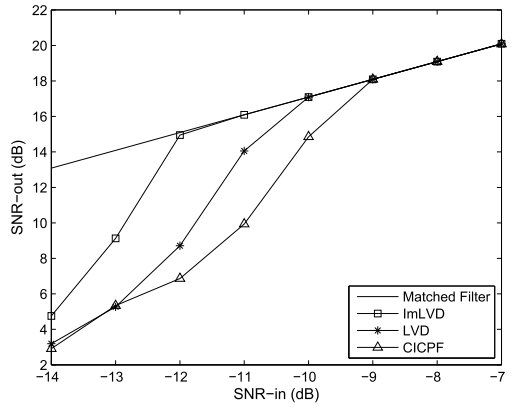

FIGURE 2. Comparison of the anti-noise performance under noisy mono-component LFM signal.

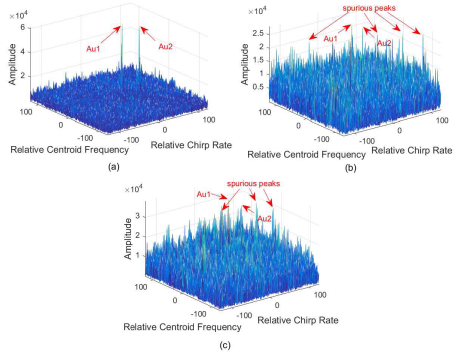

FIGURE 3. Comparison of the anti-noise performance under noisy multi-component LFM signals. (a) Result of the ImLVD. (b) Result of the LVD. (c) Result of the CICPF.

centroid frequency, and chirp rate are set as follows: $A_1 = 1$, $f_1 = 4$ Hz, $\gamma_1 = 16$ Hz/s, $f_s = 128$Hz, and $N = 256$. The input SNRs are SNR $\in [-14 : -7]$ dB.

It is easily seen from Fig. 2, when $\text{SNR}_{\text{in}} \geq -12$ dB, the SNR_{out} of ImLVD is close to that of the Matched filter. Thus, the threshold of ImLVD is -12 dB. For the LVD and CICPF, the thresholds SNR_{in} are -10 dB and -9 dB, respectively. Results in Fig. 2 show that, the anti-noise ability of ImLVD is better than that of the LVD and CICPF. That is because, by using the improved parameter selection criterion for the ImLVD, the noise correlation is decreased effectively which is beneficial to improve the anti-noise performance.

2) MULTI-COMPONENT LFM SIGNALS

Assume two components, the parameters of first component are the same as the mono-component LFM signal case. The parameters of the second component are: $A_2 = 1, f_2 = 8$ Hz, and $\gamma_2 = 8$ Hz/s. The sampling frequency f_s is 128 Hz. The effective signal length is equal to 256. The signals are contaminated with the complex white Gaussian noise with the $\text{SNR}_{\text{in}} = -10$ dB. In this paper, we use the multi-component analysis method which is the same as that presented in [34].

In Fig. 3, Au1 and Au2 denote the self-terms. We can see from Fig. 3 that the true peaks of LVD and CICPF are immersed in the noise, and the energy of the spurious peaks

TABLE 1. Computational cost.

Algorithm	Computational Cost
ImLVD	$O((N+L_{CZT})^2\log_2(N+L_{CZT}))$
LVD	$O((NL_{CZT})^2\log_2(NL_{CZT}))$
CICPF	$O((NL_{CZT})^3)$

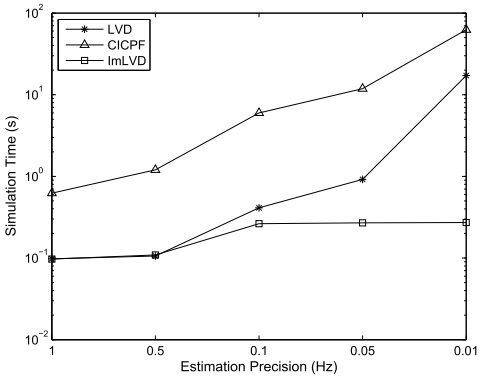

FIGURE 4. Simulation time.

approaches or exceeds that of the true peaks. Thus, it is hard to detect the LFM signals. For the ImLVD, the energy of the true peaks is much higher than that of the noise. The results in Fig. 3 can reflect the high anti-noise performance of the ImLVD under noisy multicomponent LFM signals.

B. COMPUTATIONAL COMPLEXITY ANALYSIS

In this subsection, the computational complexity analysis of ImLVD, LVD, and CICPF is described. Assume the frequency number of ISFT of coarse estimation operation is equal to N, and the estimation precision of centroid frequency and chirp rate is $f_s/(NL_{CZT})$.

The main operations of ImLVD consists of PSIAF, ISFT, FFT, and CZT. The computational complexity of them are $O(N)$, $O((N+L_{CZT})^2\log_2(N+L_{CZT}))$, $O(N^2\log_2 N)$, and $O((N+L_{CZT}/2)^2\log_2(N+L_{CZT}/2))$. Thus, computational complexity of ImLVD is $O((N+L_{CZT})^2\log_2(N+L_{CZT}))$. For the LVD, the computation cost is $O((NL_{CZT})^2\log_2(NL_{CZT}))$ [28]. For the CICPF, the computation cost is $O((NL_{CZT})^3)$ [27]. The computational costs of the ImLVD, LVD, and CICPF are listed in Table 1.

Table 1 shows that the computational complexity of ImLVD is lower than that of LVD and CICPF methods. Based on the analysis in III-B, to improve estimation precision, L_{CZT} should be increased when N is unchanged. When L_{CZT} increases, the computational complexity of ImLVD is almost no increase, but the computational complexities of LVD and CICPF are rapidly increasing.

The average simulation times of the ImLVD, LVD, and CICPF are shown in Fig. 4 under different estimation precision. The simulation results are obtained by using the R2016b MATLAB and the computer with an Intel Core i5-6200U CPU (2.40 GHz), 8 GB memory. Parameters of the LFM signal is the same with the mono-component LFM signal case under $SNR_{in} = 0$ dB.

It is easily seen from Fig. 4 that the average simulation time of ImLVD is almost unchanged with the estimation precision becoming higher, and it is less than that of the other two methods. Moreover, for the LVD and the CICPF, the average simulation times increase very quickly. For the ImLVD, we can see that when precision is 1 Hz and 0.5 Hz, the simulation times are less than other precision conditions, because when the precision requirement is not high, we just need to perform the coarse estimation operation.

V. CONCLUSION

In this paper, based on the LVD, we propose an improved method named ImLVD to analyze mono- and multi-component LFM signals. For the ImLVD, by using the double scale estimation strategy, the amount of calculation is effectively reduced, especially for estimating high precision parameters. By using the ISFT operator, the scale operation is implemented, and the coupling, which affects the performance, is removed. Based on the improved parameter selection criterion, the proposed method can achieve superior anti-noise performance. The numerical simulations demonstrate the superiority of ImLVD method about anti-noise performance and computational cost. In the future, we mainly focus on the development of the high-order version of the ImLVD for the general polynomial-phase signals.

APPENDIX

In order to demonstrate the cross-term cannot accumulate as the self-term in (10), the characteristics of $Q_{cross}(f_{t_{new}}, f_\tau)$ is analyzed in this Appendix. Based on the analysis method utilized in [44], we consider two LFM signals to formulate the cross-term problem arising from multicomponent LFM signals, which is represented as

$$s_m(t) = A_1 \exp\left(j2\pi f_1 t + j\pi\gamma_1 t^2\right) + A_2 \exp\left(j2\pi f_2 t + j\pi\gamma_2 t^2\right). \quad (27)$$

With analysis of the characteristics of the cross-term, $Q_{cross}(f_{t_{new}}, f_\tau)$ can be divided into two parts which is represented as

$$Q_{cross} = Q_{cross,1} + Q_{cross,2}, \quad (28)$$

where

$$\begin{aligned} &Q_{cross,1} \\ &= \mathrm{FT}_\tau[\mathrm{ISFT}_t[s_{m,1}(t+\frac{D+\tau}{2})s^*_{m,2}(t-\frac{D+\tau}{2})]] \\ &= \mathrm{FT}_\tau[\mathrm{ISFT}_t[A_1\exp[j2\pi f_1(t+\frac{D+\tau}{2})+j\pi\gamma_1(t+\frac{D+\tau}{2})^2] \\ &\quad \times A_2\exp[-j2\pi f_2(t-\frac{D+\tau}{2})-j\pi\gamma_2(t-\frac{D+\tau}{2})^2]]] \\ &= \mathrm{FT}_\tau[\mathrm{ISFT}_t[A_1A_2 \\ &\quad \times\exp[j2\pi(f_1+f_2)\frac{D+\tau}{2}+j\pi(\gamma_1+\gamma_2)(D+\tau)t] \\ &\quad \times\exp[j2\pi(f_1-f_2)t+j\pi(\gamma_1-\gamma_2)(t^2+(\frac{D+\tau}{2})^2)]]] \end{aligned} \quad (29)$$

and

$$\begin{aligned} &Q_{cross,2} \\ &= \mathrm{FT}_\tau[\mathrm{ISFT}_t[s_{m,2}(t+\frac{D+\tau}{2})s^*_{m,1}(t-\frac{D+\tau}{2})]] \\ &= \mathrm{FT}_\tau[\mathrm{ISFT}_t[A_2\exp[j2\pi f_2(t+\frac{D+\tau}{2})+j\pi\gamma_2(t+\frac{D+\tau}{2})^2] \\ &\quad \times A_1\exp[-j2\pi f_1(t-\frac{D+\tau}{2})-j\pi\gamma_1(t-\frac{D+\tau}{2})^2]]] \\ &= \mathrm{FT}_\tau[\mathrm{ISFT}_t[A_1A_2 \\ &\quad \times\exp[j2\pi(f_1+f_2)\frac{D+\tau}{2}+j\pi(\gamma_1+\gamma_2)(D+\tau)t] \\ &\quad \times\exp[j2\pi(f_2-f_1)t+j\pi(\gamma_2-\gamma_1)(t^2+(\frac{D+\tau}{2})^2)]]]. \end{aligned} \quad (30)$$

It is easily seen from (29) and (30) that, only when $f_1 = f_2$ and $\gamma_1 = \gamma_2$, $Q_{cross,1}$ and $Q_{cross,2}$ can be accumulated as peaks which are becoming

$$Q_{cross,1} = \mathrm{FT}_\tau[\mathrm{ISFT}_t[A_1A_2 \times\exp[j2\pi f_1(D+\tau)+j2\pi\gamma_1(D+\tau)t]]] \quad (31)$$

and

$$Q_{cross,2} = \mathrm{FT}_\tau[\mathrm{ISFT}_t[A_1A_2 \times\exp[j2\pi f_1(D+\tau)+j2\pi\gamma_1(D+\tau)t]]]. \quad (32)$$

Substituting (31) and (32) into (28),

$$Q_{cross} = 2\times\mathrm{FT}_\tau[\mathrm{ISFT}_t[A_1A_2 \times\exp[j2\pi f_1(D+\tau)+j2\pi\gamma_1(D+\tau)t]]]. \quad (33)$$

Equation (33) shows that the form of cross-term is the same as the self-term. Thus, by using the proposed method, the cross-term cannot be accumulated as spurious peaks in the CFCR domain.

REFERENCES

[1] F. Wen, Z. Zhang, K. Wang, G. Sheng, and G. Zhang, "Angle estimation and mutual coupling self-calibration for ULA-based bistatic MIMO radar," *Signal Process.*, vol. 144, pp. 61–67, Mar. 2018.
[2] H. Huang, J. Yang, H. Huang, Y. Song, and G. Gui, "Deep learning for super-resolution channel estimation and doa estimation based massive MIMO system," *IEEE Trans. Veh. Technol.*, vol. 67, no. 9, pp. 8549–8560, Sep. 2018.
[3] Y. Wang, M. Liu, J. Yang, and G. Gui, "Data-driven deep learning for automatic modulation recognition in cognitive radios," *IEEE Trans. Veh. Technol.*, vol. 68, no. 4, pp. 4074–4077, Apr. 2019.
[4] L. Wan, X. Kong, and F. Xia, "Joint range-Doppler-angle estimation for intelligent tracking of moving aerial targets," *IEEE Internet Things J.*, vol. 5, no. 3, pp. 1625–1636, Jun. 2018.
[5] F. Wen, J. Shi, and Z. Zhang, "Direction finding for bistatic MIMO radar with unknown spatially colored noise," *Circuits, Syst., Signal Process.*, pp. 1–13, Oct. 2019, doi: 10.1007/s00034-019-01260-5.
[6] F. Wen, Z. Zhang, and G. Zhang, "Joint DOD and DOA estimation for bistatic MIMO radar: A covariance trilinear decomposition perspective," *IEEE Access*, vol. 7, no. 1, pp. 53273–53283, 2019.
[7] X. Wang, L. Wan, M. Huang, C. Shen, and K. Zhang, "Polarization channel estimation for circular and non-circular signals in massive MIMO systems," *IEEE J. Sel. Topics Signal Process.*, vol. 13, no. 5, pp. 1001–1016, Sep. 2019.
[8] M. Portnoff, "Time-frequency representation of digital signals and systems based on short-time Fourier analysis," *IEEE Trans. Acoust., Speech, Signal Process.*, vol. ASSP-28, no. 1, pp. 55–69, Feb. 1980.

[9] F. Hlawatsch and G. F. Boudreaux-Bartels, "Linear and quadratic time-frequency signal representations," *IEEE Signal Process. Mag.*, vol. 9, no. 2, pp. 21–67, Apr. 1992.

[10] F. Zhang, Y. Q. Chen, and G. Bi, "Adaptive harmonic fractional Fourier transform," *IEEE Signal Process. Lett.*, vol. 6, no. 11, pp. 45–48, May 1999.

[11] V. Katkovnik, "A new form of the Fourier transform for time-varying frequency estimation," *Signal Process.*, vol. 47, no. 2, pp. 187–200, 1995.

[12] T. A. C. M. Claasen and W. F. G. Mecklenbrauker, "The Wigner distribution—A tool for time-frequency signal analysis. II. Discrete time signals," *Philips J. Res.*, vol. 35, no. 3, pp. 217–250, 1980.

[13] Z.-C. Zhang, "Unified Wigner–Ville distribution and ambiguity function in the linear canonical transform domain," *Signal Process.*, vol. 114, pp. 45–60, Sep. 2015.

[14] J. C. Wood and D. T. Barry, "Radon transformation of time-frequency distributions for analysis of multicomponent signals," *IEEE Trans. Signal Process.*, vol. 42, no. 11, pp. 3166–3177, Nov. 1994.

[15] S. Barbarossa, "Analysis of multicomponent LFM signals by a combined Wigner–Hough transform," *IEEE Trans. Signal Process.*, vol. 43, no. 6, pp. 1511–1515, Jun. 1995.

[16] A. Y. Erdogan, T. O. Gulum, L. Durak-Ata, T. Yildirim, and P. E. Pace, "FMCW signal detection and parameter extraction by cross Wigner–Hough transform," *IEEE Trans. Aerosp. Electron. Syst.*, vol. 53, no. 1, pp. 334–344, Feb. 2017.

[17] M. Wang, A. K. Chan, and C. K. Chui, "Linear frequency-modulated signal detection using Radon-ambiguity transform," *IEEE Trans. Signal Process.*, vol. 46, no. 3, pp. 571–586, Mar. 1998.

[18] Y. Sun and P. Willett, "Hough transform for long chirp detection," *IEEE Trans. Aerosp. Electron. Syst.*, vol. 38, no. 2, pp. 553–569, Apr. 2002.

[19] G. Bi, X. Li, and C. M. S. See, "LFM signal detection using LPP-Hough transform," *Signal Process.*, vol. 91, no. 6, pp. 1432–1443, 2011.

[20] A. Bouchikhi, A. O. Boudraa, J. C. Cexus, and T. Chonavel, "Analysis of multicomponent LFM signals by Teager Huang–Hough transform," *IEEE Trans. Aerosp. Electron. Syst.*, vol. 50, no. 2, pp. 1222–1233, Apr. 2014.

[21] L. B. Almeida, "The fractional Fourier transform and time-frequency representations," *IEEE Trans. Signal Process.*, vol. 42, no. 11, pp. 3084–3091, Nov. 1994.

[22] L. Zheng and D. Shi, "Maximum amplitude method for estimating compact fractional Fourier domain," *IEEE Signal Process. Lett.*, vol. 17, no. 3, pp. 293–296, Mar. 2010.

[23] P. O'Shea, "A new technique for instantaneous frequency rate estimation," *IEEE Signal Process. Lett.*, vol. 9, no. 8, pp. 251–252, Aug. 2002.

[24] P. Wang and J. Yang, "Multicomponent chirp signals analysis using product cubic phase function," *Digit. Signal Prog.*, vol. 16, no. 6, pp. 654–669, 2006.

[25] P. Wang, H. Li, I. Djurović, and B. Himed, "Integrated cubic phase function for linear FM signal analysis," *IEEE Trans. Aerosp. Electron. Syst.*, vol. 46, no. 3, pp. 963–977, Jul. 2010.

[26] J. Su, H.-H. Tao, X. Rao, J. Xie, and X.-L. Guo, "Coherently integrated cubic phase function for multiple LFM signals analysis," *Electron. Lett.*, vol. 51, no. 5, pp. 411–413, 2015.

[27] D. Li, M. Zhan, J. Su, H. Liu, X. Zhang, and G. Liao, "Performances analysis of coherently integrated CPF for LFM signal under low SNR and its application to ground moving target imaging," *IEEE Trans. Geosci. Remote Sens.*, vol. 55, no. 11, pp. 6402–6419, Nov. 2017.

[28] X. Lv, G. Bi, C. Wan, and M. Xing, "Lv's distribution: Principle, implementation, properties, and performance," *IEEE Trans. Signal Process.*, vol. 59, no. 8, pp. 3576–3591, Aug. 2011.

[29] S. Luo, G. Bi, X. Lv, and F. Hu, "Performance analysis on Lv distribution and its applications," *Digit. Signal Process.*, vol. 23, no. 3, pp. 797–807, 2013.

[30] Y. Li, T. Su, J. Zheng, and X. He, "ISAR imaging of targets with complex motions based on modified Lv's distribution for cubic phase signal," *IEEE J. Sel. Topics Appl. Earth Observ. Remote Sens.*, vol. 8, no. 10, pp. 4775–4784, Oct. 2015.

[31] L. Yang, L. Zhao, S. Zhou, and G. Bi, "Sparsity-driven SAR imaging for highly maneuvering ground target by the combination of time-frequency analysis and parametric Bayesian learning," *IEEE J. Sel. Topics Appl. Earth Observ. Remote Sens.*, vol. 10, no. 4, pp. 1443–1455, Apr. 2017.

[32] W. Yu, W. Su, and H. Gu, "Fast method for radar maneuvering target detection and motion parameter estimation," *Multidimens. Syst. Signal Process.*, vol. 29, no. 4, pp. 1411–1425, 2018.

[33] Y. Zhao, S. Han, J. Yang, L. Zhang, H. Xu, and J. Wang, "A novel approach of slope detection combined with Lv's distribution for Airborne SAR imagery of fast moving targets," *Remote Sens.*, vol. 10, no. 5, p. 764, 2018.

[34] J. Zheng, H. Liu, and Q. H. Liu, "Parameterized centroid frequency-chirp rate distribution for LFM signal analysis and mechanisms of constant delay introduction," *IEEE Trans. Signal Process.*, vol. 65, no. 24, pp. 6435–6447, Dec. 2017.

[35] L. Rabiner, R. Schafer, and C. Rader, "The chirp *z*-transform algorithm," *IEEE Trans. Audio Electroacoust.*, vol. AU-17, no. 2, pp. 86–92, Jun. 1969.

[36] F. Jing, C. Zhang, Y. Wang, S. Jiao, and W. Si, "QFM signals parameters estimation based on double scale two dimensional frequency distribution," *IEEE Access*, vol. 7, pp. 4496–4505, 2019.

[37] P. Wang, H. Li, I. Djurovic, and B. Himed, "Performance of instantaneous frequency rate estimation using high-order phase function," *IEEE Trans. Signal Process.*, vol. 58, no. 4, pp. 2415–2421, Apr. 2010.

[38] F. Wen, X. Xiong, J. Su, and Z. Zhang, "Angle estimation for bistatic MIMO radar in the presence of spatial colored noise," *Signal Process.*, vol. 134, pp. 261–267, May 2017.

[39] F. Wen, X. Xiong, and Z. Zhang, "Angle and mutual coupling estimation in bistatic MIMO radar based on PARAFAC decomposition," *Digit. Signal Process.*, vol. 65, pp. 1–10, Jun. 2017.

[40] H. Wang, L. Wan, M. Dong, K. Ota, and X. Wang, "Assistant vehicle localization based on three collaborative base stations via SBL-based robust DOA estimation," *IEEE Internet Things J.*, vol. 6, no. 3, pp. 5766–5777, Jun. 2019.

[41] F. Wen, C. Mao, and G. Zhang, "Direction finding in MIMO radar with large antenna arrays and nonorthogonal waveforms," *Digit. Signal Process.*, vol. 94, pp. 75–83, Nov. 2019.

[42] X. Lv, M. Xing, C. Wan, and S. Zhang, "ISAR imaging of maneuvering targets based on the range centroid Doppler technique," *IEEE Trans. Image Process.*, vol. 19, no. 1, pp. 141–153, Jan. 2010.

[43] W. Cui, S. Wu, J. Tian, D. Liu, and S. Wu, "Parameter estimation for maneuvering targets with complex motion via scaled double-autocorrelation transform," *Digit. Signal Process.*, vol. 59, pp. 31–48, Dec. 2016.

[44] J. Zheng, T. Su, L. Zhang, Q. H. Liu, and W. Zhu, "ISAR imaging of targets with complex motion based on the chirp rate–quadratic chirp rate distribution," *Trans. Geosci. Remote Sens.*, vol. 52, no. 11, pp. 7276–7289, Nov. 2014.

[45] J. Zheng, T. Su, H. Liu, G. Liao, Z. Liu, and Q. H. Liu, "Radar high-speed target detection based on the frequency-domain deramp-keystone transform," *IEEE J. Sel. Topics Appl. Earth Observ. Remote Sens.*, vol. 9, no. 1, pp. 285–294, Jan. 2016.

YU WANG was born in 1990. She received the B.S. and Ph.D. degrees in electronics and information engineering from Harbin Engineering University, in 2013 and 2019, respectively. She is currently a Lecturer with the College of Electronics and Information, Shenyang Aerospace University, Shenyang, China. Her research interests include blind souse separation and radar signal processing.

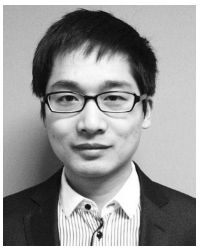

KE WANG was born in Hubei, China, 1988. He received the B.S. degree in automation engineering from the Hubei University of Technology, Wuhan, China, 2010, and the Ph.D. degree from the College of Electronic Information and Control Engineering, Beijing University of Technology, in 2016. Since 2016, he has been with the Electronic and Information School, Yangtze University, China, where he is currently a Lecturer. His research interests include mobile robot and computer vision.

FULONG JING was born in 1990. He received the B.S. and Ph.D. degrees in electronics and information engineering from Harbin Engineering University, in 2013 and 2019, respectively. He is currently with the Shenyang Aircraft Design and Research Institute. His research interests include radar signal processing and array signal processing.

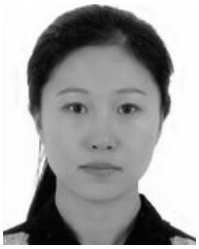

XIAOYU LAN (M'15) received the B.S. and Ph.D. degrees from the College of Information and Communication Engineering, Harbin Engineering University, Harbin, China, in 2008 and 2012, respectively. Since 2013, she has been an Associate Professor with the College of Electronics and Information, Shenyang Aerospace University, Shenyang, China. Her current research interests are mainly in the areas of array signal processing, wireless sensor networks, and signal processing in MIMO systems and its applications.

YAN ZOU received the B.S. and Ph.D. degrees from the College of Information and Communication Engineering, Harbin Engineering University, Harbin, China, in 2013 and 2019, respectively. He has been a Researcher with the Shenyang Aircraft Design and Research Institute, China, since 2019. His research interests include array signal processing, information fusion, and communication countermeasures.

LIANGTIAN WAN (M'15) received the B.S. and Ph.D. degrees from the College of Information and Communication Engineering, Harbin Engineering University, Harbin, China, in 2011 and 2015, respectively. From October 2015 to April 2017, he was a Research Fellow with the School of Electrical and Electrical Engineering, Nanyang Technological University, Singapore. He is currently an Associate Professor with the School of Software, Dalian University of Technology, China. He is the author of over 30 articles published in related international conference proceedings and journals. His current research interests include social network analysis and mining, big data, array signal processing, wireless sensor networks, and compressive sensing. Dr. Wan has been serving as an Associate Editor for IEEE Access and the *Journal of Information Processing Systems*.